NOTES AND CORRESPONDENCE

A Combined Wind Profiler and Polarimetric Weather Radar Method for the Investigation of Precipitation and Vertical Velocities

MICHIHIRO S. TESHIBA* AND PHILLIP B. CHILSON

School of Meteorology, and Atmospheric Radar Research Center, University of Oklahoma, Norman, Oklahoma

ALEXANDER V. RYZHKOV

Atmospheric Radar Research Center, and Cooperative Institute for Mesoscale Meteorological Studies, University of Oklahoma, and NOAA/OAR National Severe Storms Laboratory, Norman, Oklahoma

TERRY J. SCHUUR

Cooperative Institute for Mesoscale Meteorological Studies, University of Oklahoma, and NOAA/OAR National Severe Storms Laboratory, Norman, Oklahoma

ROBERT D. PALMER

School of Meteorology, and Atmospheric Radar Research Center, University of Oklahoma, Norman, Oklahoma

(Manuscript received 18 December 2007, in final form 24 November 2008)

ABSTRACT

A method is presented by which combined S-band polarimetric weather radar and UHF wind profiler observations of precipitation can be used to extract the properties of liquid phase hydrometeors and the vertical velocity of the air through which they are falling. Doppler spectra, which contain the air motion and/or fall speed of hydrometeors, are estimated using the vertically pointing wind profiler. Complementary to these observations, spectra of rain drop size distribution (DSD) are simulated by several parameters as related to the DSD, which are estimated through the two polarimetric parameters of radar reflectivity (Z_H) and differential reflectivity (Z_{DR}) from the scanning weather radar. These DSDs are then mapped into equivalent Doppler spectra (fall speeds) using an assumed relationship between the equivolume drop diameter and the drop's terminal velocity. The method is applied to a set of observations collected on 11 March 2007 in central Oklahoma. In areas of stratiform precipitation, where the vertical wind motion is expected to be small, it was found that the fall speeds obtained from the spectra of the rain DSD agree well with those of the Doppler velocity estimated with the profiler. For those cases when the shapes of the Doppler spectra are found to be similar in shape but shifted in velocity, the velocity offset is attributed to vertical air motion. In convective rainfall, the Doppler spectra of the rain DSD and the Doppler velocity can exhibit significant differences owing to vertical air motions together with atmospheric turbulence. Overall, it was found that the height dependencies of Doppler spectra measured by the profiler combined with vertical profiles of Z, Z_{DR}, and the cross correlation (ρ_{HV}) as well as the estimated spectra of raindrop physical terminal fall speeds from the polarimetric radar provide unique insight into the microphysics of precipitation. Vertical air motions (updrafts/downdrafts) can be estimated using such combined measurements.

1. Introduction

Midlatitude mesoscale convective systems (MCSs) have been the focus of countless studies over the past years. These storm systems are usually characterized by a leading convective line followed by a region of trailing

* Current affiliation: Weathernews Inc., Chiba, Japan.

Corresponding author address: Michihiro S. Teshiba, School of Meteorology, University of Oklahoma, 120 David L. Boren Blvd., Rm. 5900, Norman, OK 73072-7307.
E-mail: teshiba@arrc.ou.edu

DOI: 10.1175/2008JTECHA1102.1

stratiform precipitation. Often there is a distinct transition zone between these two regions, characterized by reduced values of the radar reflectivity. Evaporative cooling of the precipitation contributes to a mesoscale downdraft below the freezing level and to the formation of a cold pool and gust front, which can trigger additional convective cells. The system is typically fed by a rear inflow jet. Some of the studies of midlatitude MCSs include Smull and Houze (1987), Biggerstaff and Houze (1991, 1993), Bluestein et al. (1994), Brandes (1990), Houze et al. (1990), and Hane and Jorgensen (1995). Obtaining reliable estimates of the vertical velocity within MCSs is necessary to construct a three-dimensional model of the flow patterns within these storms; however, the measurements are not always easy to obtain.

Although many different methods for estimating the vertical wind component within MCSs have been devised and successfully implemented, we will only concentrate on those involving ground-based remote sensing technologies, namely, radar. These fall broadly into the categories of single-Doppler analysis, dual-Doppler analysis, and wind profiler techniques. There is an extensive body of literature dealing with the retrieval of wind fields using Doppler radar, but most of these studies focus on horizontal winds. The retrieval of the vertical component of the wind field is more problematic. As we will show, each of the proposed methods suffers from inherent limitations.

For a single-Doppler weather radar, one can estimate the vertical component of the three-dimensional wind using a velocity–azimuth display (VAD) (Browning and Wexler 1968), volume velocity processing (VVP) (Waldteufel and Corbin 1979), or other similar techniques. Each uses the assumption that the wind field is uniform, or varies at most linearly, across the volume scanned by the radar. Then, some form of mass continuity equation is invoked to get the vertical air motion. In addition to these single-Doppler scanning methods, there have also been attempts to extract vertical air motion estimates from data obtained while the radar is oriented vertically (Rogers 1964; Joss and Waldvogel 1970; Zawadzki et al. 2005). Here, a particular form of the drop size distribution (DSD) and the relation between equivolume drop diameters and their terminal fall speeds are assumed. Then, using a radar reflectivity–rainfall rate (Z–R) relationship, the expected mean fall speed of the observed precipitation can be estimated from the radar reflectivity factor. The difference between the expected mean fall speed and the observed vertical Doppler velocity gives the vertical air motion.

By incorporating data from two weather radars, we can begin to directly investigate the three-dimensional dynamic and thermodynamic features of storm systems using a dual-Doppler radar analysis (Armijo 1969; Lhermite 1970). This method has been extensively used in the past to study the three-dimensional wind field within MCSs. However, the ''three dimensional'' qualifier most often means that estimates of the horizontal wind in three dimensions are retrieved as opposed to the three-dimensional wind vector itself. A few examples of studies that do use dual-Doppler data to retrieve the vertical wind field include Houze et al. (1989), Biggerstaff and Houze (1993), and Braun and Houze (1994). Recently, Shapiro and Mewes (1999) have presented a new formulation for retrieving the three-dimensional wind field using dual-Doppler radar data. Mewes and Shapiro (2002) have specifically discussed the problems associated with estimating the vertical velocity field using dual-Doppler measurements and that some form of constraining equation must be introduced. In the case of Mewes and Shapiro (2002), the anelastic vorticity equation is invoked as that constraint.

The main objective of this paper is to present a new method of investigating combined observations of precipitation from polarimetric weather radars and wind profilers. Through this method, properties of liquid phase hydrometeors together with estimates of vertical air motion through which the particles are falling are retrieved. Data from the polarimetric weather radar are used together with an empirically based model to find estimates of the drop size distribution for the rain. These data are used in conjunction with Doppler spectra from a vertically pointing wind profiler and an assumed relationship between equivolume drop diameter and its terminal fall speed to calculate the vertical component of the wind. The mathematical framework and underlying assumptions incorporated into the technique are provided in section 2. To test the method, an experiment was conducted during which an MCS was observed (see section 3). The resulting data are analyzed and presented in section 4, and some of the inferred properties of precipitation associated with the MCS can be found in section 5. Finally, the conclusions are outlined in section 6.

2. Background and mathematical framework

Wind profilers are specifically designed to measure the vertical and horizontal components of the wind field aloft. However, it is generally difficult to distinguish between contributions of precipitation and vertical air motion using a single UHF wind profiler. If, however, the wind profiler operates at sufficiently long wavelengths, for example, VHF, both precipitation and clear-air returns contribute to the backscattered signal and can often be distinguished in the Doppler spectrum. Then, it becomes trivial to measure the vertical wind; in these

cases, precipitation properties can also be investigated (Fukao et al. 1985; Wakasugi et al. 1986; Rajopadhyaya et al. 1994; Lucas et al. 2004). In some studies, two wind profilers of different wavelengths (UHF and VHF) are deployed (Gage et al. 1999; Cifelli et al. 2000; Schafer et al. 2002). Then, the UHF and VHF signals can be used primarily to measure the precipitation and clear-air backscatter, respectively. If one is solely interested in measuring the fall speed of the hydrometeors, then it may be possible to simply assume that the vertical component of the wind field is negligibly small, as is often the case in stratiform precipitation (Williams 2002).

Unique opportunities to explore the characteristics of rain microphysics can be achieved using complementary data from wind profilers and polarimetric weather radars (e.g., May et al. 2001, 2002; May and Keenan 2005). In a joint project involving the National Oceanic and Atmospheric Administration's National Severe Storms Laboratory (NOAA NSSL) and the University of Oklahoma (OU), such measurements of precipitation are being pursued. One of the wind profilers used in the study is a UHF radar operated through the OU Atmospheric Radar Research Center (ARRC) and is located at the Kessler Farm Field Laboratory (KFFL) (Chilson et al. 2007). Another wind profiler available for the study, which is also located at KFFL, is part of the NOAA Profiler Network (NPN) and regularly produces estimates of the three-dimensional wind profile (Benjamin et al. 2004). The NPN profiler also operates at UHF. Polarimetric radar data are obtained using the research platform Weather Surveillance Radar-1988 Doppler (WSR-88D; KOUN) operated by NOAA NSSL. Polarimetric radar data, such as those provided with KOUN, have been shown to be an effective resource for precipitation studies (e.g., Ryzhkov et al. 2005a,b; Scharfenberg et al. 2005).

Radar reflectivity (Z_H), differential radar reflectivity (Z_{DR}), and cross correlation (ρ_{HV}) from the polarimetric weather radar are used to provide information regarding hydrometeors within the radar sampling volume (Straka et al. 2000). If the DSD of raindrops is assumed to follow a constrained gamma distribution, which is determined by two parameters, then these parameters can be estimated from the measurements of Z_H and Z_{DR} (e.g., Zhang et al. 2001; Brandes et al. 2004; Cao et al. 2008). The characteristics of hydrometeors below and around the freezing level are studied by examining the DSDs estimated using the polarimetric radar together with the Doppler spectra measured with the ARRC profiler operating in a vertically pointing mode. Horizontal wind data are provided by the NPN profiler. An additional source of weather radar data is the WSR-88D located near Oklahoma City (KTLX).

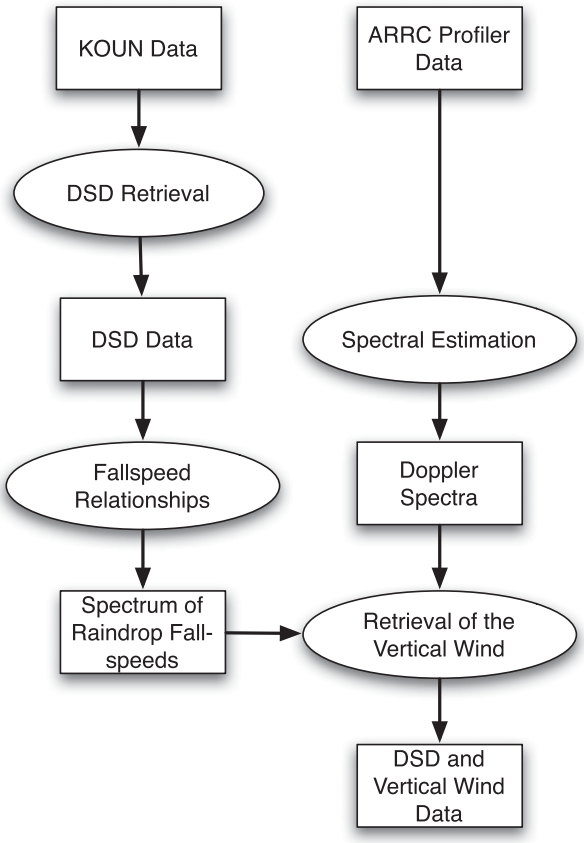

FIG. 1. Schematic of the data flow and algorithms used for the radar signal processing and retrieval of the vertical wind. Squares and ovals denote data files and data processing steps, respectively.

The wind retrieval algorithm used in the present study uses estimates of the DSD from polarimetric weather radar data together with a knowledge of the terminal fall speed of precipitation in air. As described below, Doppler spectra of terminal fall speeds for raindrops are estimated using a polarimetric DSD retrieval. Comparing the retrieved spectra of terminal fall speeds with the spectra directly measured by the wind profiler allows us to estimate the vertical velocity of the air motion. A schematic depicting the approach is shown in Fig. 1. It is assumed that all precipitation is liquid (no ice). Therefore, we focus our attention below the melting layer.

a. DSD estimating algorithm

The method of estimating DSD data from polarimetric weather radar observations used in the present study is mainly based on the work of Cao et al. (2008). It applies to liquid precipitation and assumes that the underlying DSD follows a constrained gamma distribution as given by

$$N(D) = N_o D^{\mu} \exp(-\Lambda D), \tag{1}$$

where D is the equivolume diameter of the raindrops and the parameters μ and Λ are related to one another through the empirical equation (Cao et al. 2008)

$$\mu = \mu'(\Lambda) + C\Delta Z_{\rm DR}, \tag{2}$$

where

$$\mu'(\Lambda) = -0.0201\Lambda^2 + 0.902\Lambda - 1.718, \tag{3}$$

$$\Delta Z_{\rm DR} = Z_{\rm DR} - Z_{\rm DR}^{(a)}, \tag{4}$$

$$Z_{\rm DR}^{(a)} = 10^{f(Z_H)}, \tag{5}$$

$$f(Z_H) = -5.01710 \times 10^{-4} Z_H^2 + 0.07401 Z_H - 2.0122, \tag{6}$$

and

$$C = 2. \tag{7}$$

In the above equations, Z_H and $Z_{\rm DR}$ are expressed in decibels and the coefficients were determined empirically. The parameter μ is constrained to be within the interval [0, 6]. The intercept parameter N_o can be estimated through the comparison between the radar reflectivity from the radar and rain DSD. The radar reflectivity is given by

$$Z_H = \int N(D) D^6 \, dD. \tag{8}$$

Using this procedure, it has been possible to obtain estimates of the DSDs from the polarimetric weather radar observations.

b. Vertical velocity retrieval algorithm

Having estimated DSDs from the polarimentric observations, the next step is to map these data into equivalent Doppler spectra (fall speeds of the hydrometeors) using an assumed relationship between the drop diameter and the corresponding terminal fall velocity. This can be expressed mathematically as

$$S_n(w) = \frac{D^6 N(D)}{Z_h} \frac{dD}{dw}, \tag{9}$$

where Z_h is given in linear units (mm^6 m^{-3}), $S_n(w)$ is the "simulated" normalized Doppler spectrum (e.g., Doviak and Zrnić 1993), and $N(D)$ is the DSD found from Z_H and $Z_{\rm DR}$. Here, it has been assumed that the raindrop fall speeds are related to their diameters according to

$$\begin{aligned} w(D) &= \left(\frac{\rho_o}{\rho}\right)^{0.4} (3.78 D^{0.67}) && D \le 3 \text{ mm}, \\ &= \left(\frac{\rho_o}{\rho}\right)^{0.4} [9.65 - 10.3 \ \exp(-0.6D)] && D > 3 \text{ mm}, \end{aligned} \tag{10}$$

where ρ and ρ_o are the atmospheric densities aloft and at the surface, respectively. The value of the exponent (0.4) was found empirically by Foote and du Toit (1969). Although several different fall speed relations can be found in the literature, it has been shown by Kanofsky and Chilson (2008) that the estimated Doppler spectrum is relatively insensitive to which particular relationship is chosen.

The simulated Doppler spectrum calculated using (9) represents the fall speeds that the drops would experience in still air. The Doppler spectra obtained from the wind profiler, on the other hand, contain contributions from both the particle fall speeds and the air motion. By comparing the two sets of spectra (those estimated from the ARRC profiler and those simulated from the KOUN data) and assuming that the assumptions that went into the retrievals are correct, it is possible to estimate the velocity of the bulk vertical air motion. That is, for those cases when the two sets of Doppler spectra are found to be similar in shape but shifted in velocity, the velocity offset is attributed to the vertical air motion (see Fig. 1).

c. Synthesized time–height intensity plot

Wind profilers typically probe the atmosphere aloft using a combination of three or more vertically and near-vertically oriented beams. This sampling geometry is chosen to provide the best estimates of the three-dimensional wind components aloft. As such, wind profilers provide data as a function of height at regular time intervals. The resulting backscattered power, for example, can then be displayed using a time–height intensity plot. Similar plots showing velocity and turbulence data can also be constructed.

For the purpose of the present study, the polarimetric weather radar (KOUN) was operated in a range–height indicator (RHI) mode in the direction of the wind profiler. It is convenient to present the polarimetric data collected over the profiler in a time–height plane. These observations can be directly compared with measurements from the profiler. Examples of such processing and further discussion are provided below.

3. Experimental setup and data collection

To test the method of combining data from polarimetric weather radars and wind profilers, a special series of measurements were conducted in central Oklahoma. In this section we provide a brief summary of the instruments used and discuss how they were configured. Two wind profilers were operated at the OU Kessler Farm Field Laboratory, which is located approximately 30 km south of the OU campus. During precipitation

events, the atmosphere above the KFFL site was probed using two S-band weather radars (see section 3b).

a. Kessler Farm Field Laboratory

The Kessler Farm Field Laboratory is a 140-ha property that is maintained and operated by OU. KFFL provides an ideal location for complementary measurements to those obtained using the two WSR-88Ds used in this study, since it is close enough to ensure good resolution but far enough to be outside of the region of ground clutter. Furthermore, KFFL offers the necessary infrastructure to support the deployment of several instruments, which are needed for the study of precipitation and the validation of radars. For example, OU's School of Meteorology operates a two-dimensional video disdrometer and network of tipping-bucket rain gauges at KFFL. Additionally, KFFL is host to several other atmospheric measurement programs, which provide atmospheric measurements that can be used for targeted precipitation studies. Those programs relevant to this discussion are the Department of Energy Atmospheric Radiation Measurement Program (DOE ARM) and the Oklahoma Mesonet.

b. Instrumentation

The two primary instruments used during this study were an S-band polarimetric weather radar and a UHF wind profiler (or boundary layer radar). The weather radar is a prototype polarimetric WSR-88D used for research and development purposes and is operated by NOAA NSSL (Doviak et al. 2000). The wind profiler is maintained and operated by the OU ARRC group (Chilson et al. 2007). For the remainder of this discussion, these two instruments will be simply referred to as the KOUN and ARRC profilers, respectively.

KOUN was designed and built as a test platform for the development and testing of algorithms intended to improve upon current quantitative precipitation estimation (QPE) methodologies. With the exception of its polarimetric capabilities, the technical specifications of KOUN are similar to the other WSR-88D systems currently deployed across the United States and in other parts of the world. That is, KOUN is an 11-cm radar with a beamwidth of 1° and a minimum pulse width of 1.57 μs (235 m in range resolution). Using KOUN, the effectiveness of polarimetric weather radar observations has been successfully demonstrated (e.g., Ryzhkov et al. 2005b). Indeed, the success of KOUN has been sufficient to convince NOAA officials to sanction the upgrade of the national network of WSR-88Ds within the United States to include polarization diversity (Saffle et al. 2007).

The ARRC profiler operates at 915 MHz (corresponding to a wavelength of 33 cm). The beamwidth of the wind profiler is 9°, and the beam can be directed vertically or electronically steered along four oblique directions having zenith angles of 22° (Carter et al. 1995). The minimum range resolution for the radar is 60 m, but a more typical mode of operation uses a range resolution of 100–200 m. For the present study, the ARRC profiler was operated using only a vertical beam.

Given the beamwidths, the range resolutions, and the separation between KOUN and the ARRC profiler, the sampling volumes of the two instruments match relatively well near the surface. The ground separation between KOUN and the ARRC profiler is approximately 30 km. Taking KOUN's lowest elevation angle of 0.5° as an example, we find that the resulting angular resolution and height above ground level at the location of the ARRC profiler are 500 and 250 m, respectively. The height of 250 m is approximately equal to the lowest sampling volume of the ARRC profiler as configured for this experiment. The angular resolution of the ARRC profiler at a height of 250 m is 40 m. It should be noted here that the two radars have been calibrated independently. That is, the values for the radar reflectivity reported in section 4 can be taken as independent parameters.

Two additional radars are used in support of the present study: the WSR-88D (KTLX), located near Oklahoma City; and one of the radars in the NOAA Profiler Network, located at KFFL. KTLX provides continuous plan position indicator (PPI) scans and provides the overall structure of precipitating systems that pass over KFFL. Such data are useful when diagnosing the mesoscale environment in which the precipitation forms. The NPN is dedicated to providing height profiles of the three-dimensional wind vector and the virtual temperature at several sites within the central United States (Benjamin et al. 2004). Regrettably, the NPN UHF radars are not capable of providing Doppler spectra. As we discuss below, Doppler spectra from profiling radars provide a means of investigating the structure and evolution of precipitation as a function of time and height. Therefore, this radar is primarily used for wind comparisons.

4. Observations of a mesoscale convective system

In this section, we demonstrate the utility of synthesizing time–height intensity plots from RHI data and the applicability of the vertical wind–estimating algorithm described above by presenting observations of a storm system that passed over central Oklahoma. On 11 March 2007, a low pressure system moved from west

to east across Oklahoma, which resulted in the formation of a large mesoscale convective system. The system was characterized by the formation of a line of strong convective clouds along a cold front, which extended in the north–south direction. The west side of the convective line was dominated by a region of trailing stratiform rainfall (see Fig. 2).

A typical MCS is associated with three distinct types of precipitation: convective, stratiform, and a transition between convective and stratiform portions (e.g., Smull and Houze 1987; Biggerstaff and Houze 1993; Braun and Houze 1994). Hydrometeors that form in the convective region are carried rearward by the MCSs' midlevel, front-to-rear flow; bridge the transition zone region; and then grow by vapor deposition in the stratiform region broad mesoscale updraft. Intense aggregation and melting as they fall through the freezing level result in a layer of enhanced reflectivity that is known as the radar bright band.

Both the ARRC and NPN profilers provided continuous measurements as the system passed over KFFL. The ARRC profiler beam was directed vertically and the time and height resolutions during the observations were 20 s and 200 m, respectively. Figure 3 shows time–height intensity plots of the radar reflectivity, Doppler velocity, and spectrum width from 1100 to 1300 UTC for the ARRC profiler. Negative velocity values indicate motion toward the radar. The observations indicate convection in the leading edge of the storm (before 1130 UTC) and in the period between 1150 and 1210 UTC. The precipitation was predominantly stratiform after 1210 UTC. The spectrum width data shown in the bottom panel of Fig. 3 contain contributions from atmospheric turbulence as well as the dispersion of fall speeds resulting from the DSD of hydrometeors. Another factor influencing the spectrum width is beam broadening. To quantify this effect, we examine the measurements from the NPN.

Spectral broadening effects become relevant when we later compare the Doppler spectra from the ARRC profiler with the synthesized Doppler spectra from KOUN. The increase of spectral width due to beam broadening experienced by a radar depends on its beamwidth and the magnitude of the wind component transverse to the beam. This contribution is given by Nastrom (1997) and Gossard et al. (1998) as

$$\sigma^2 = \frac{V_t^2 \Theta_a^2}{2 \log 4}, \tag{11}$$

where V_t is the magnitude of the transverse wind (horizontal wind in this case) and Θ_a is the one-way half-power half-width of the beam, expressed in radians.

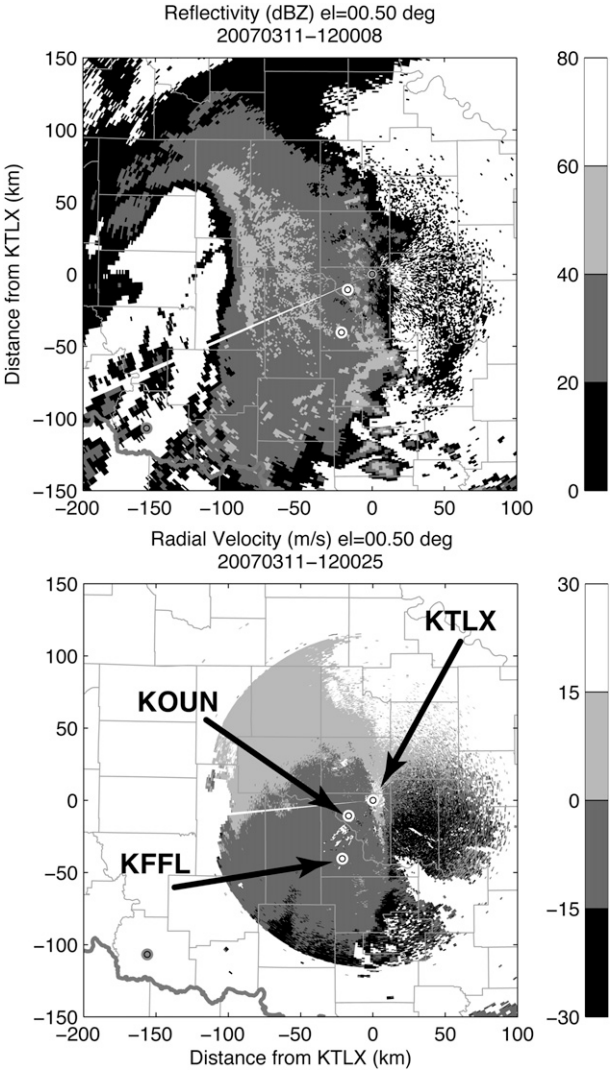

FIG. 2. Horizontal distribution of radar reflectivity and Doppler velocity as observed by KTLX WSR-88D for a 0.5° elevation angle at 1200 UTC on 11 Mar 2007.

For the ARRC profiler, $\Theta_a = 9°/\sqrt{2}\,(\pi/180°) = 0.111$ rad. Wind data from the NPN profiler are available during the time of this event every 6 min and extend in height up to 16 km. Figure 4 shows four height profiles of the horizontal wind speed observed during the storm. The times were chosen to correspond to the four distinct precipitation signatures selected for detailed study in section 5. The first three profiles are generally less than 10 m s^{-1} below 4 km. This corresponds to a contribution to the spectral width of 0.7 m s^{-1}. For the 1230 UTC profile, the horizontal wind speed is approximately 15 m s^{-1} between 2 and 4 km. The corresponding contribution to the spectral width is 1 m s^{-1}.

The temperature profile from the sounding data collected for Norman, OK (OUN), at 1200 UTC on

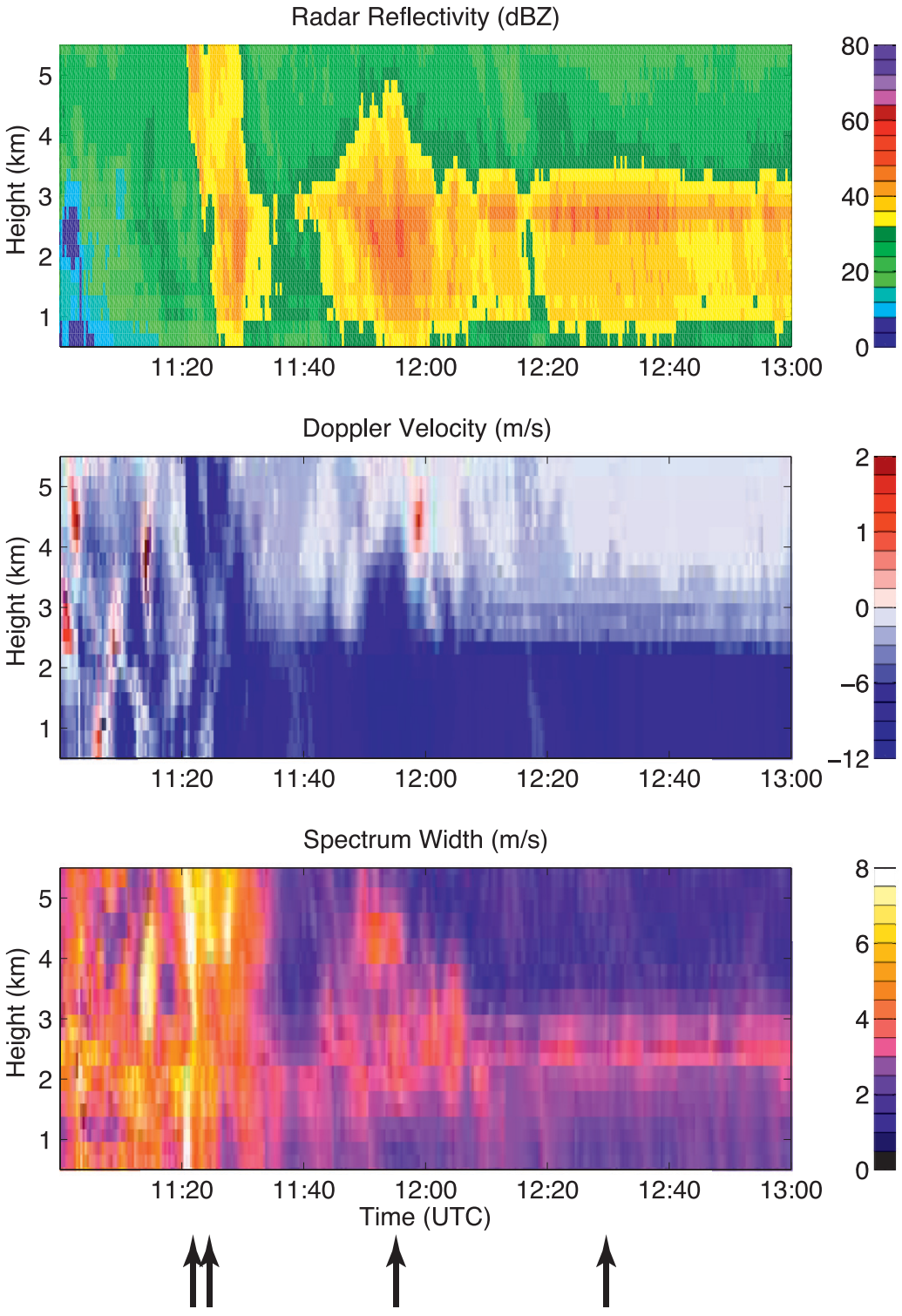

FIG. 3. Time–height cross sections of radar reflectivity, Doppler velocity, and spectrum width observed with the OU profiler. Heights are given relative to MSL. Arrows indicate those times selected for further analysis and presented in section 5.

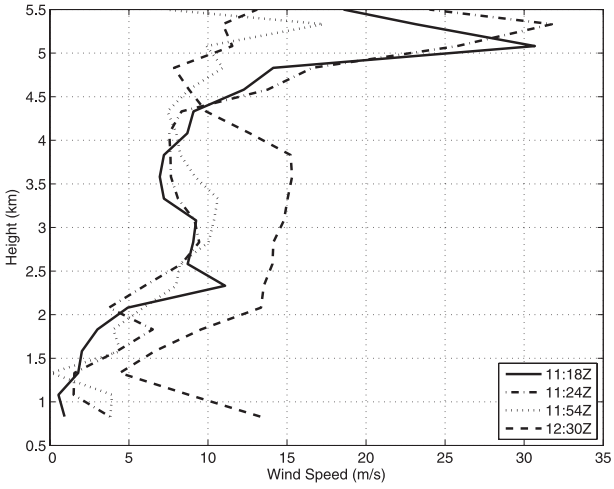

FIG. 4. Height profiles of the horizontal wind speed observed with the NOAA 404-MHz profiler at 1118 (solid line), 1124 (dotted–dashed line), 1154 (dotted line), and 1230 UTC (dashed line). Heights are given relative to MSL.

11 March (not shown) indicates that the freezing level was located at approximately 3 km MSL. This is consistent with the observations from the ARRC profiler. After 1210 UTC, the presence of a bright band can be seen in the reflectivity plot at a height of approximately 3 km. Furthermore, there is a large change in the magnitude of the observed Doppler velocities near this height. Note that the polarimetric DSD estimation was only applied to those KOUN data well below the freezing level. The sounding data were also used to adjust the calculated terminal fall speeds of the raindrops with height.

KOUN was operated in an RHI scanning mode in the direction of the two wind profilers (~191° in azimuth) during the MCS event. RHI data were collected from 1058 to 1444 UTC. The vertical angular resolution of the polarimetric data was 0.1°, which corresponds to height increments of approximately 50 m above KFFL. The RHI composite plot of Z_H, Z_{DR}, and ρ_{HV} for an azimuth angle of 191° at time 1200 UTC is shown in Fig. 5. In the stratiform rain region (which passed over KFFL after approximately 1210 UTC), high reflectivity values associated with the bright band are found at a height of around 2.5 km. The differential reflectivity is roughly uniform in height below a height of 2 km, and the general shape of the DSDs are considered to be relatively similar during that period.

Using the method discussed above, a synthesized time–height composite plot of Z_H, Z_{DR}, and ρ_{HV} was constructed from the RHI data over KFFL (Fig. 6). The features in the synthesized time–height panel of the radar reflectivity factor agree qualitatively with those shown in Fig. 3 from the ARRC profiler. Recall that the two radars were calibrated independently of one another. The bottom panel in Fig. 6 shows the vertical velocity data, which were retrieved using the algorithm introduced in the previous section. As discussed below, these wind measurements agree qualitatively with earlier reports showing the wind field structures associated with midlatitude MCSs (Houze et al. 1989; Biggerstaff and Houze 1993; Braun and Houze 1994). In section 5 we present some examples of the combined measurements from KOUN and the ARRC profiler in more detail.

Although not a classic example of an MCS, the storm system observed on 11 March does generally follow the patterns associated with an MCS. A line of convective clouds formed along the cold front and stratiform clouds formed on the western side of the convective region. In the convective region around 1124 UTC, a moderately strong updraft up to 5 m s^{-1} was observed; shortly thereafter a region of strong reflectivity (more than 50 dBZ) was found to extend to a height of at least 5.5 km, indicative of convective squall line. The squall line is marked by enhanced values of Z_{DR} from a height of 2–2.5 km to the surface, indicative of large raindrops. Consistent with these observations, downdrafts of approximately 2 m s^{-1} are observed below 1.5 km. The transition from dry snow to wet snow at the top of the melting layer is marked by a rapid increase of Z_{DR} and a decrease of ρ_{HV}. In the presence of downdrafts associated with increased precipitation between 1150 and 1200 UTC, such a transition occurs at the lower height levels, as Fig. 6 indicates. The stratiform portion of the storm corresponds to those observations made after 1210 UTC. In this region the bright band is well formed and the downdrafts are weak (approximately 1 m s^{-1} or less). Overall, the retrieved vertical velocity field exhibits features typical of an MCS.

In an attempt to test the robustness of the method, the similarity of these Doppler spectra of the KOUN weather radar and ARRC profiler have been compared against each other. Figure 7 shows the root-mean-square error (RMSE) of these Doppler spectra in decibels at each height and time as it relates to the reflectivity of the KOUN radar. As shown in Eq. (10), the terminal fall speed of raindrops asymptotically approaches a value of 9.6 m s^{-1}; therefore, only portions of the Doppler spectra could be correctly estimated. Equation (10) has been obtained based on ground-base observations; however, in this paper, we considered these portions of the spectra to have been correctly estimated, and the RMSE is calculated based on these estimates. Since fluctuations in the vertical wind differ according to the type of rainfall being observed, the data have been

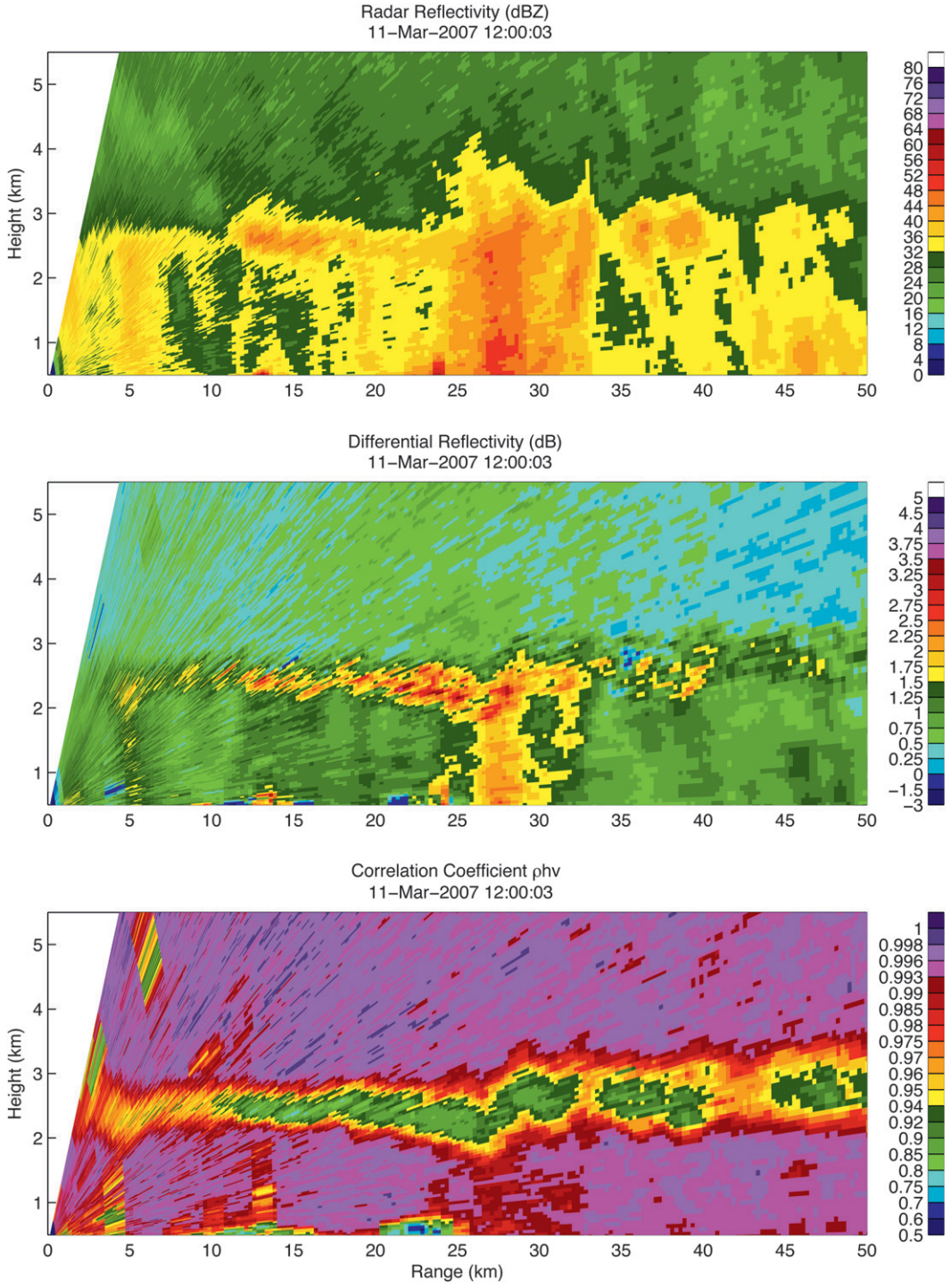

FIG. 5. Range–height cross sections of Z_H, Z_{DR}, and ρ_{HV} of KOUN at 1200 UTC. KFFL is located 30 km in range from KOUN.

grouped according to convective (1058–1130 UTC), transition (1130–1204 UTC), and stratiform (1204–1445 UTC) regions. Heights for the calculation were all taken below 1.77 km MSL. As shown in Fig. 7, the RMSE is generally below 3 dB for all cases. In the stratiform rainfall region, the RMSE is approximately 1 dB. There is no clear reflectivity dependence for the RMSE calculated for any of the cases; therefore, it

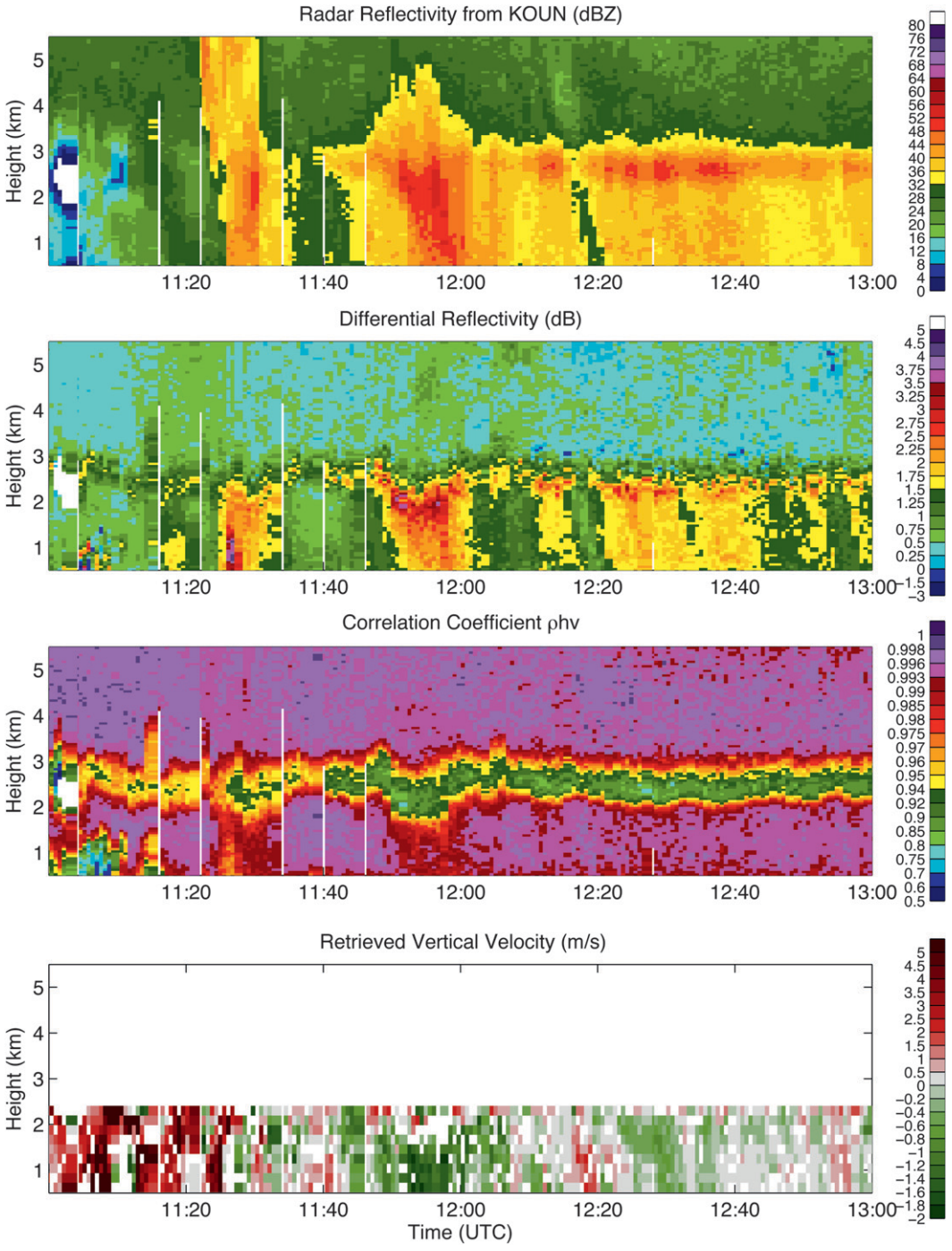

FIG. 6. Time–height cross sections of radar reflectivity, differential reflectivity, correlation coefficient over the KFFL observed with the KOUN polarimetric radar and retrieved vertical wind component. Heights are given relative to MSL.

appears as though the retrieval technique can be applied over a wide range of rainfall events. Of course, additional observations will be needed to substantiate this claim.

5. Retrieved precipitation microphysics

Here, we present typical height profiles of data retrieved using KOUN and the ARRC profiler during

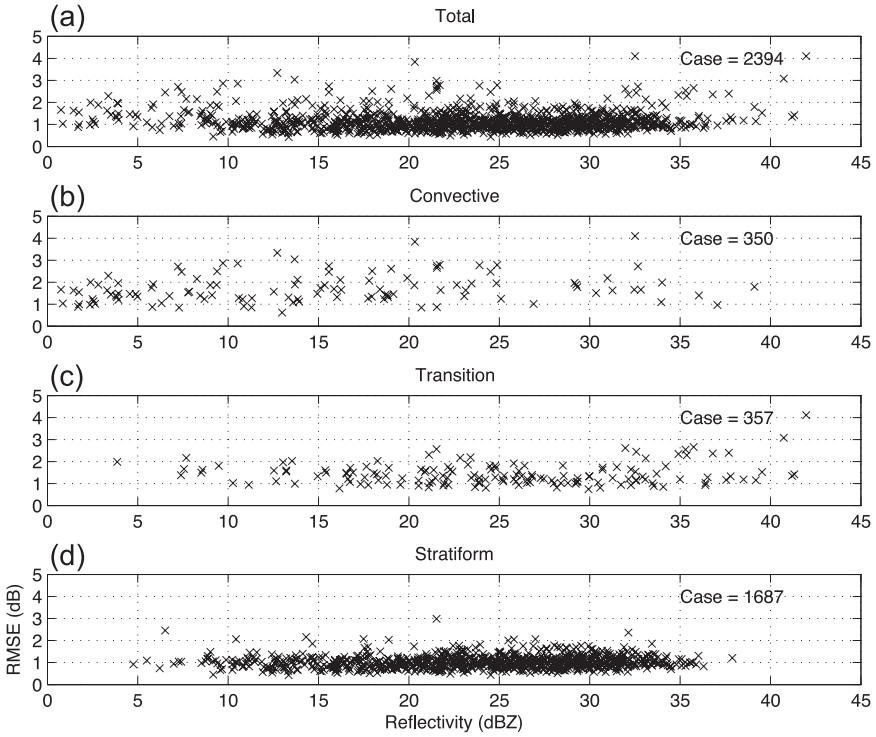

FIG. 7. RMSE of the two Doppler spectra corresponding to data for KOUN and the ARRC profiler as related to the reflectivity of KOUN: (a) all cases, (b) convective region, (c) transition region, and (d) stratiform region. Points in the scatterplots were calculated for every time and height believed to represent measurements of liquid phase precipitation.

different phases of the MCS as it passed over KFFL. Properties of hydrometeors are found through the polarimetric variables of Z, Z_{DR}, and ρ_{HV}, and temperature profiles at the KOUN sounding station, as shown in Straka et al. (2000). For each of the selected cases, vertical profiles of Z, Z_{DR}, and ρ_{HV} together with the Doppler spectra from KOUN and the profiler are shown. The Doppler spectra have all been normalized to their peak values. For the sake of comparison, the vertical spacing of KOUN spectral data has been matched to the range resolution of the ARRC profiler (200 m). The four examples presented below were selected as being characteristic of the different stages of cloud and precipitation development within the MCS. A brief speculative account of the underlying physical processes contributing to the observations is provided for each of the four cases. Data from other available observations are still being studied to construct a more comprehensive analysis of the 11 March MCS. Although the explanations of the examples provided below remain to be verified, they do form a plausible and self-consistent picture of the MCS. Similar results can be found, for example, in Houze et al. (1989), Biggerstaff and Houze (1993), Bluestein et al. (1994), and Braun and Houze (1994). Furthermore, these examples illustrate the utility of combined profiler and polarimetric weather radar observations to study precipitation.

a. Early development of precipitation aloft—Heights exceeding 4 km (1122 UTC)

The presence of large graupel is manifested by large terminal velocities measured by the profiler and high radar reflectivity (well over 40 dBZ) at altitudes above 4 km (see Fig. 8). The presence of strong downdrafts is not likely at such heights, and substantial negative velocities above 4 km are associated with the fall of graupel/small hail (Straka et al. 2000). The hydrometeors in the lower portion of the cloud are quite different than those aloft, as demonstrated by the sudden drop in the magnitude of Z_H and the fall velocities below 4 km. Most likely, small-sized dry and melting graupel was dominant within the height interval between 2.3 and 3.4 km. It seems that there is no connection between this small-sized graupel and the large graupel/hail aloft. In other words, these two species of graupel might have been advected from different parts of the cloud. Raindrops with relatively small sizes below the melting layer most likely resulted from melting

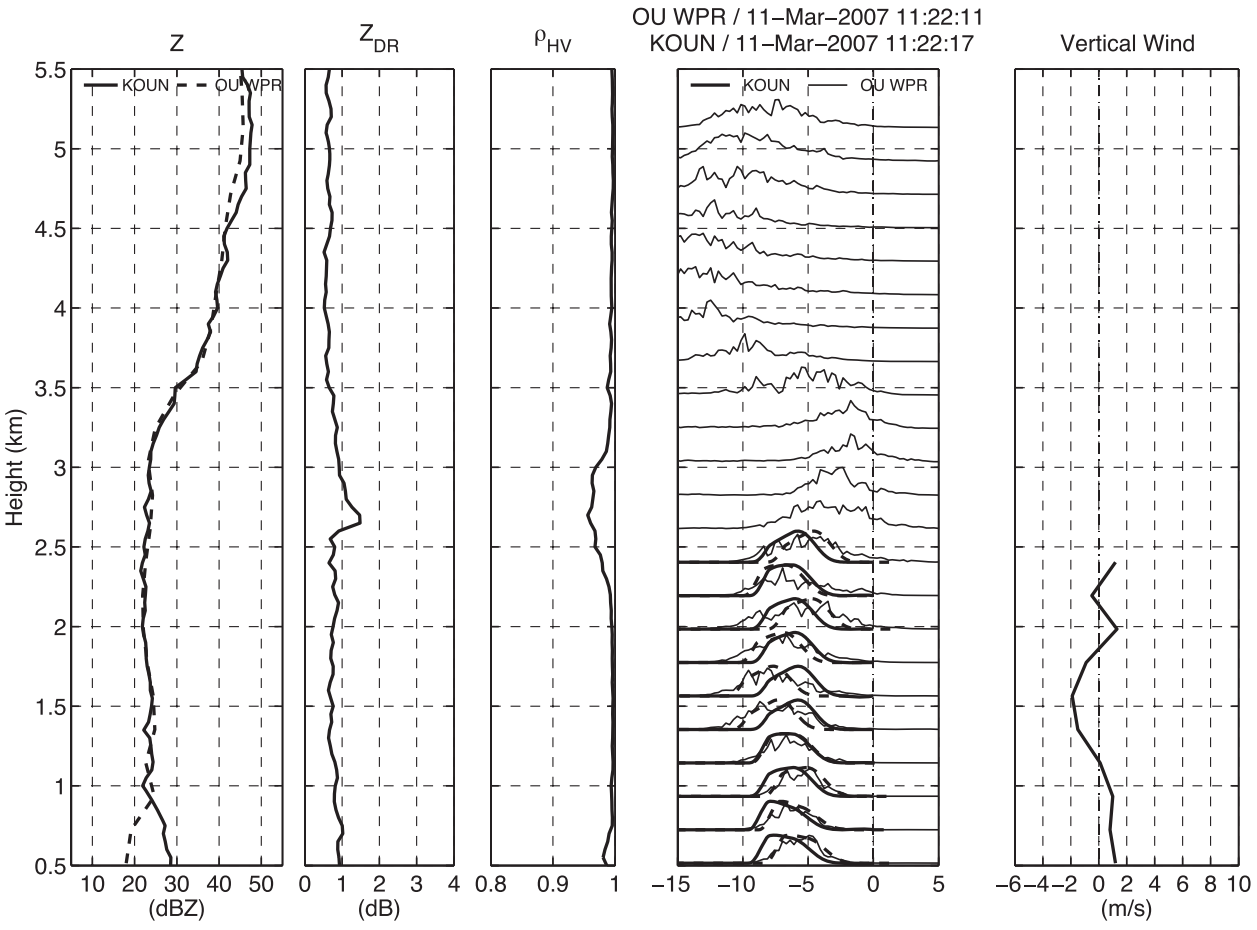

FIG. 8. Vertical profiles of Z, Z_{DR}, and ρ_{HV}; spectra of the particle fall speeds and Doppler velocity; and retrieved vertical wind component at 1122 UTC. The radar reflectivity profiles of KOUN and the profiler are shown in the same axis. The spectra of estimated (KOUN), measured (profiler), and fitted velocities are indicated in dark solid, light solid, and dashed lines, respectively. The retrieved spectra are only shown for heights up to 2.5 km (well below the freezing level). Heights are given relative to MSL.

graupel. Another possible explanation is that at 1122 UTC, large graupel/hail formed aloft and did not have time to fall below the 4-km level. Tilting of the reflectivity core might be an alternative explanation. Note that the melting layer is marked by the decrease in ρ_{HV} and by the rapid change of Z_{DR} within the height interval between 2.5 and 3 km. The Z_{DR} maximum and ρ_{HV} minimum are relatively weak in the melting layer, which also points to the melting of smaller-sized graupel.

b. Strong updraft at lower levels (1124 UTC)

At this time, the updraft portion of the system passed over the profiler (see Fig. 9). The updraft at the levels 0.5–2.5 km is revealed by the striking differences between the spectra of vertical velocities estimated from KOUN and those measured by the profiler. The strength of the updraft in this case is approximately 6 m s^{-1}. Another indication of the updraft below 2.5 km is the combination of low Z_H (of approximately 30 dBZ) and relatively high Z_{DR} (up to 2 dB at this time and above 4 dB 1–2 min later), which points to substantial size sorting of raindrops; that is, raindrops with terminal velocities less than 6 m s^{-1} do not fall through the updraft. At higher levels, the situation is quite similar to the one previously discussed (1122 UTC in section 5a), but Z_H is lower and the corresponding terminal fall speeds are lower.

c. Convective downdraft (1155 UTC)

A classic signature of a convective downdraft within the main precipitation shaft is observed at this time (see Fig. 10). A bulk of precipitation descends, hence larger Z_H is observed at lower levels below 3 km. Convective rain below the melting layer originates from melting graupel/small hail, which has relatively high terminal velocities immediately above the melting layer. Near

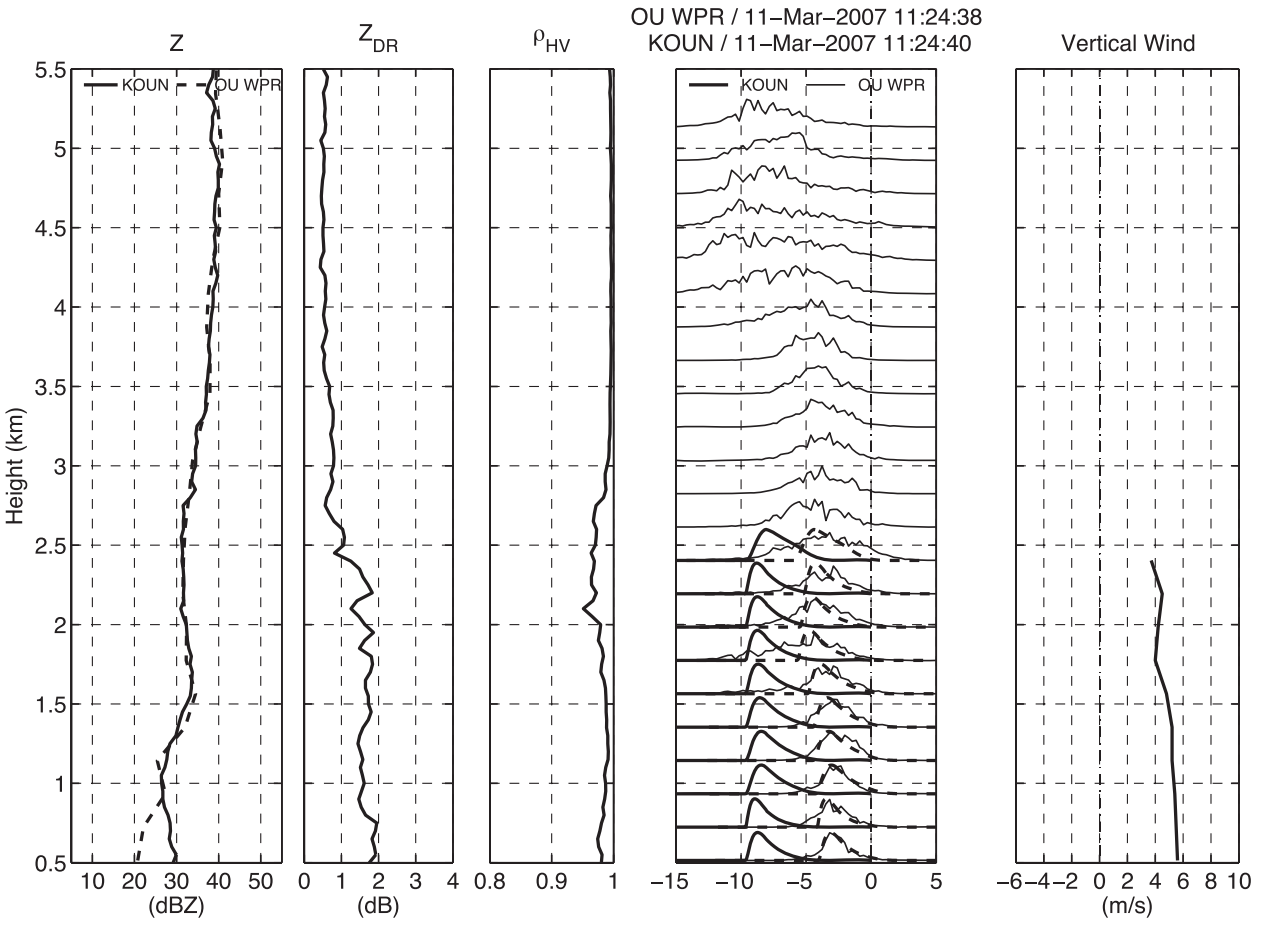

FIG. 9. Same as in Fig. 8, but for 1124 UTC.

the ground, the difference between modal values of KOUN and the profiler spectra corresponds to a downdraft of approximately 2 m s^{-1}, which is likely generated by melting graupel/hail. The downdraft combined with cooling due to melting results in a depression of the melting layer height (it is pushed closer to the ground), as indicated by the vertical profiles of Z_{DR} and ρ_{HV} (see Fig. 6). As a result, complete melting of graupel/hail occurs at a height slightly above 1.5 km (with the freezing level at 3 km in the ambient air).

d. Stratiform rain—Vertical motions are negligible (1231 UTC)

These data indicate a classic signature of the bright band generated by melting snowflakes (see Fig. 11). There is no graupel aloft, and the difference between the terminal velocities of aggregated snowflakes above the freezing level and the raindrops below is large. The minimum in the vertical profile of ρ_{HV} is deeper, narrower, and higher compared to the situation of convective downdraft. The spectra of vertical velocities estimated from the polarimetric radar and those measured with the wind profiler agree remarkably well. This may serve as indirect evidence of the high quality of polarimetric DSD estimation used in this study. We must keep in mind that the Doppler spectra from the ARRC profiler are subject to turbulence. This is not the case for the synthesized Doppler spectra from KOUN.

6. Conclusions

Investigations of the microphysical processes of precipitation formation can be greatly facilitated through the combined use of wind profiler and polarimetric weather radar data (May et al. 2001, 2002; May and Keenan 2005). When oriented vertically, Doppler spectra from the wind profiler can be used to directly measure the vertical velocities of the sampled precipitation particles. The height dependencies of Doppler spectra measured by the profiler combined with the vertical profiles of Z_H, Z_{DR}, and ρ_{HV} as well as the estimated spectra of raindrop physical terminal fall speeds from

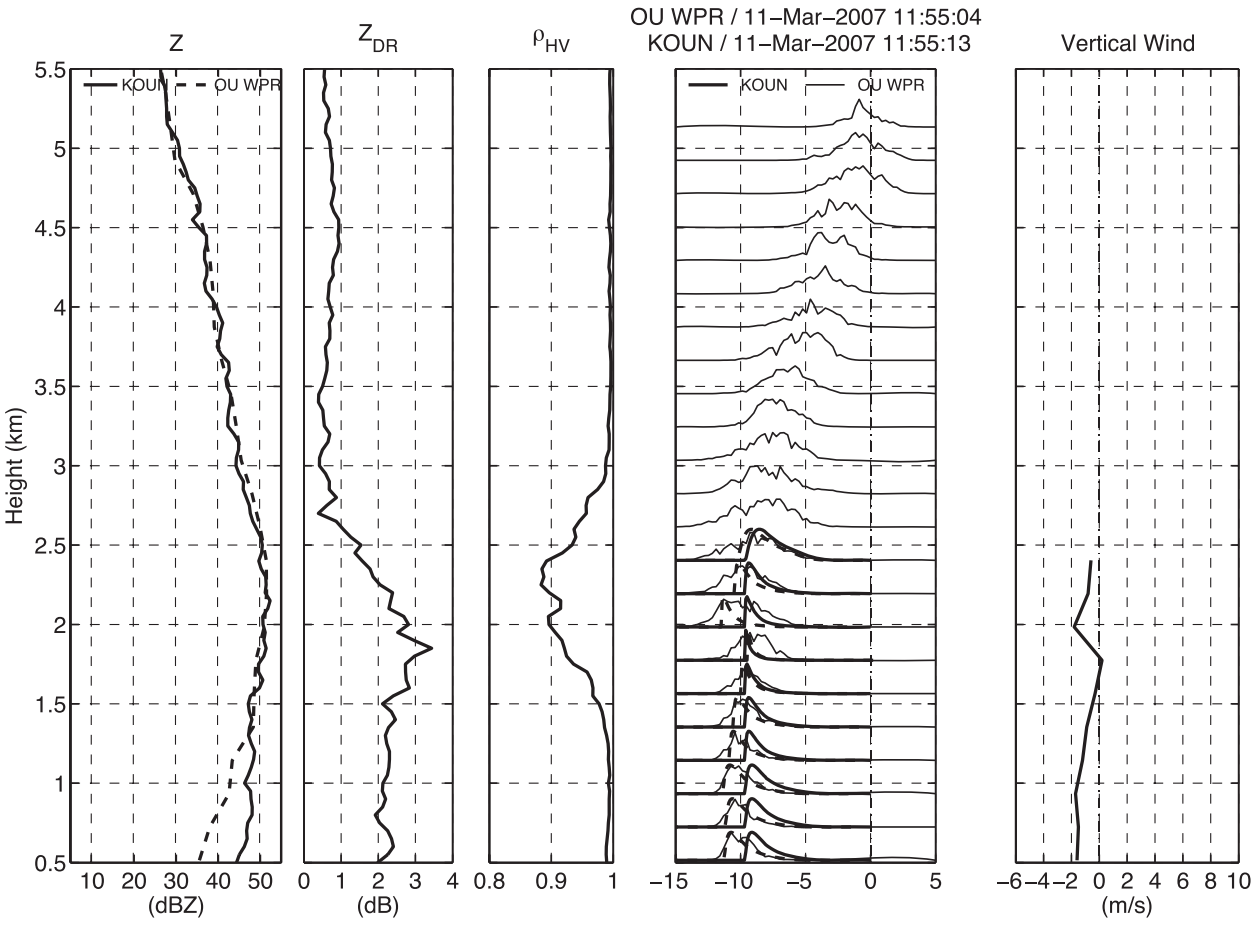

FIG. 10. Same as in Fig. 8, but for 1155 UTC.

polarimetric radar provide unique insight into the microphysics of precipitation. For example, these measurements facilitate a detailed study of precipitation processes in and around the melting layer. For this particular case of raindrops, the polarimetric observables Z_H and Z_{DR} are used to estimate the underlying DSD based on a constrained gamma model. Then, using an assumed fall-speed relationship, the DSD can be mapped into an equivalent spectrum of reflectivity-weighted vertical velocities. These data can be directly compared to the observed spectrum of particle fall velocities measured with a profiling radar. As such, vertical air motions (updrafts/downdrafts) can be estimated using the combined measurements.

The method is being implemented in central Oklahoma using data from KOUN and KTLX in conjunction with measurements from the ARRC and NPN profilers (both located at KFFL). The separation between KOUN and the two profilers is only 30 km; therefore, the sampling volumes for KOUN and the OU profiler are similar.

An example of data collected for an MCS event has been presented. In particular, four cases representative of different stages of cloud and precipitation development within the MCS have been discussed in some detail. The analysis of these data is still ongoing; however, the following examples have been shown:

- Stacked profiles of the vertical velocity spectra estimated from KOUN for raindrops show remarkable agreement with those directly measured with the ARRC profiler during stratiform precipitation when vertical air motions are negligible.
- In some cases, the spectra from KOUN and the ARRC profiler agreed well in shape but were offset in velocity, which is attributed to vertical air motion.
- Updrafts as large as 6 m s^{-1} were present near the leading edge of the MCS, which resulted in significant size sorting of the raindrops.
- Melting graupel/hail below the melting level was likely responsible for an observed convective downdraft of 2 m s^{-1}.

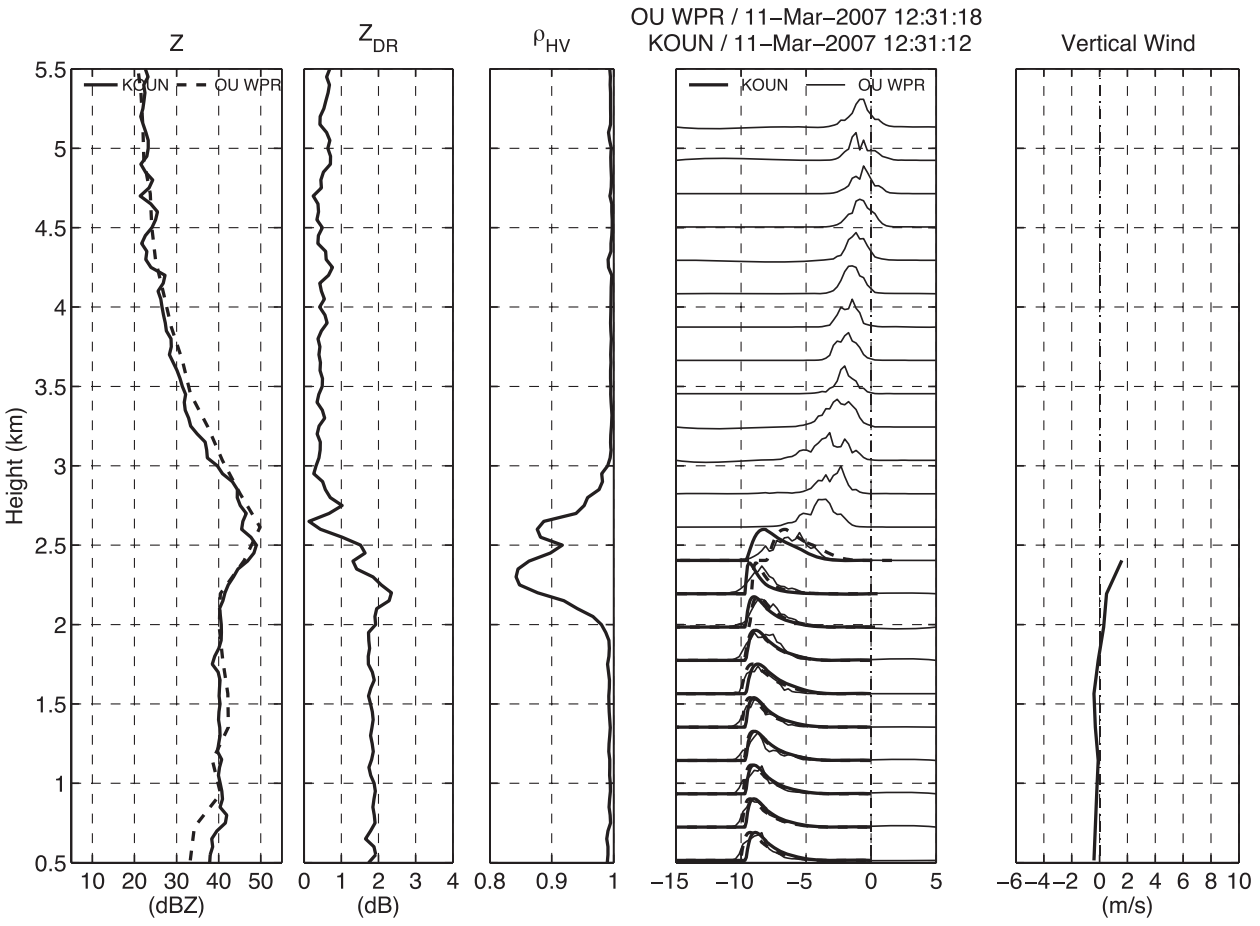

FIG. 11. Same as in Fig. 8, but for 1231 UTC.

Admittedly, the data presented here require further analysis to better understand the dynamic structure of the 11 March MCS. To this end, supporting data from the other available instrumentation will be used. Nevertheless, a plausible and self-consistent characterization of the storm event is already beginning to evolve based on the measurements that have been shown and discussed.

Acknowledgments. Funding for Alexander Ryzhkov and Terry Schuur was provided by NOAA/Office of Oceanic and Atmospheric Research under NOAA/University of Oklahoma Agreement #NA17RJ1227, U.S. Department of Commerce.

REFERENCES

Armijo, L., 1969: A theory for the determination of wind and precipitation velocities with Doppler radars. *J. Atmos. Sci.,* **26,** 570–573.

Benjamin, S. G., B. E. Schwartz, E. J. Szoke, and S. E. Koch, 2004: The value of wind profiler data in U.S. weather forecasting. *Bull. Amer. Meteor. Soc.,* **85,** 1871–1886.

Biggerstaff, M. I., and R. A. Houze, Jr., 1991: Midlevel vorticity structure of the 10–11 June 1985 squall line. *Mon. Wea. Rev.,* **119,** 3066–3079.

——, and ——, 1993: Kinematics and microphysics of the transition zone of the 10–11 June 1985 squall line. *J. Atmos. Sci.,* **50,** 3091–3110.

Bluestein, H. B., S. D. Hrebenach, C.-F. Chang, and E. A. Brandes, 1994: Synthetic dual-Doppler analysis of mesoscale convective systems. *Mon. Wea. Rev.,* **122,** 2105–2124.

Brandes, E. A., 1990: Evolution and structure of the 6–7 May 1985 mesoscale convective system and associated vortex. *Mon. Wea. Rev.,* **118,** 109–127.

——, G. Zhang, and J. Vivekanandan, 2004: Drop size distribution retrieval with polarimetric radar: Model and application. *J. Appl. Meteor.,* **43,** 461–475.

Braun, S. A., and R. A. Houze, Jr., 1994: The transition zone and secondary maximum of radar reflectivity behind a midlatitude squall line: Results retrieved from Doppler radar data. *J. Atmos. Sci.,* **51,** 2733–2755.

Browning, K. A., and R. Wexler, 1968: The determination of kinematic properties of a wind field using Doppler radar. *J. Appl. Meteor.,* **7,** 105–113.

Cao, Q., G. Zhang, E. A. Brandes, T. Schuur, A. Ryzhkov, and K. Ikeda, 2008: Analysis of video disdrometer and polarimetric radar data to characterize rain microphysics in Oklahoma. *J. Appl. Meteor. Climatol.,* **47,** 2238–2255.

Carter, D. A., K. S. Gage, W. L. Ecklund, W. M. Angevine, P. E. Johnston, A. C. Riddle, J. Wilson, and C. R. Williams, 1995: Developments in UHF lower tropospheric wind profiling at NOAA's Aeronomy Laboratory. *Radio Sci.,* **30,** 977–1001.

Chilson, P. B., G. Zhang, T. Schuur, L. M. Kanofsky, M. S. Teshiba, Q. Cao, M. V. Every, and G. Ciach, 2007: Coordinated in-situ and remote sensing precipitation measurements at the Kessler Farm Field Laboratory in central Oklahoma. Preprints, *33rd Int. Conf. on Radar Meteorology,* Cairns, Queensland, Australia, Amer. Meteor. Soc., P8A.4. [Available online at http://ams.confex.com/ams/pdfpapers/123396.pdf.]

Cifelli, R., C. R. Williams, D. K. Rajopadhyaya, S. K. Avery, K. S. Gage, and P. T. May, 2000: Drop-size distribution characteristics in tropical mesoscale convective systems. *J. Appl. Meteor.,* **39,** 760–777.

Doviak, R. J., and D. S. Zrnić, 1993: *Doppler Radar and Weather Observations*. 2nd ed. Academic Press, 562 pp.

——, V. Bringi, A. Ryzhkov, A. Zahrai, and D. Zrnić, 2000: Considerations for polarimetric upgrades to operational WSR-88D radars. *J. Atmos. Oceanic Technol.,* **17,** 257–278.

Foote, G. B., and P. S. du Toit, 1969: Terminal velocity of raindrops aloft. *J. Appl. Meteor.,* **8,** 249–253.

Fukao, S., K. Wakasugi, T. Sato, S. Morimoto, T. Tsuda, I. Hirota, I. Kimura, and S. Kato, 1985: Direct measurement of air and precipitation particle motion by very high frequency Doppler radar. *Nature,* **316,** 712–714.

Gage, K. S., C. R. Williams, W. L. Ecklund, and P. E. Johnson, 1999: Use of two profilers during MCTEX for unambiguous identification of Bragg scattering and Rayleigh scattering. *J. Atmos. Sci.,* **56,** 3679–3691.

Gossard, E. E., D. E. Wolfe, K. P. Moran, R. A. Paulus, K. D. Anderson, and L. T. Rogers, 1998: Measurement of clear-air gradients and turbulence properties with radar wind profiles. *J. Atmos. Oceanic Technol.,* **15,** 321–342.

Hane, C. E., and D. P. Jorgensen, 1995: Dynamic aspects of a distinctly three-dimensional mesoscale convective system. *Mon. Wea. Rev.,* **123,** 3194–3214.

Houze, R. A., Jr., M. I. Biggerstaff, S. A. Rutledge, and B. F. Smull, 1989: Interpretation of Doppler weather radar displays of midlatitude mesoscale convective systems. *Bull. Amer. Meteor. Soc.,* **70,** 608–619.

——, B. F. Smull, and P. Dodge, 1990: Mesoscale organization of springtime rainstorms in Oklahoma. *Mon. Wea. Rev.,* **118,** 613–654.

Joss, J., and A. Waldvogel, 1970: Raindrop size distribution and Doppler velocities. Preprints, *14th Conf. on Radar Meteorology,* Tuscon, AZ, Amer. Meteor. Soc., 153–156.

Kanofsky, L., and P. B. Chilson, 2008: An analysis of errors in drop size distribution retrievals and rain bulk parameters with a UHF wind profiling radar and a two-dimensional video disdrometer. *J. Atmos. Oceanic Technol.,* **25,** 2282–2292.

Lhermite, R. M., 1970: Dual-Doppler radar observation of convective storm circulation. Preprints, *14th Conf. on Radar Meteorology,* Tucson, AZ, Amer. Meteor. Soc., 139–144.

Lucas, C., A. D. MacKinnon, R. A. Vincent, and P. T. May, 2004: Raindrop size distribution retrievals from a VHF boundary layer profiler. *J. Atmos. Oceanic Technol.,* **21,** 45–60.

May, P. T., and T. D. Keenan, 2005: Evaluation of microphysical retrievals from polarimetric radar with wind profiler data. *J. Appl. Meteor.,* **44,** 827–838.

——, A. R. Jameson, T. D. Keenan, and P. E. Johnson, 2001: A comparison between polarimetric radar and wind profiler observations of precipitation in tropical showers. *J. Appl. Meteor.,* **40,** 1702–1717.

——, ——, ——, ——, and C. Lucas, 2002: Combined wind profiler/polarimetric radar studies of the vertical motion and microphysical characteristics of tropical sea-breeze thunderstorms. *Mon. Wea. Rev.,* **130,** 2228–2239.

Mewes, J. J., and A. Shapiro, 2002: Use of the vorticity equation in dual-Doppler analysis of the vertical velocity field. *J. Atmos. Oceanic Technol.,* **19,** 543–567.

Nastrom, G. D., 1997: Doppler radar spectral width broadening due to beamwidth and wind shear. *Ann. Geophys.,* **15,** 786–796.

Rajopadhyaya, D. K., P. T. May, and R. A. Vincent, 1994: The retrieval of ice particle size information from VHF wind profiler Doppler spectra. *J. Atmos. Oceanic Technol.,* **11,** 1559–1568.

Rogers, R. R., 1964: An extension of the *Z-R* relation for Doppler radar. Preprints, *11th Weather Radar Conf.,* Boston, MA, Amer. Meteor. Soc., 158–169.

Ryzhkov, A. V., S. E. Giangrande, and T. J. Schuur, 2005a: Rainfall estimation with a polarimetric prototype of WSR-88D. *J. Appl. Meteor.,* **44,** 502–515.

——, T. J. Schuur, D. W. Burgess, S. Giangrande, and D. S. Zrnic, 2005b: The joint polarization experiment: Polarimetric rainfall measurements and hydrometeor classification. *Bull. Amer. Meteor. Soc.,* **86,** 809–824.

Saffle, R. E., M. J. Istok, and G. S. Cate, 2007: NEXRAD product improvement—Update 2007. Preprints, *23rd Conf. of IIPS,* San Antonio, TX, Amer. Meteor. Soc., 5B.1. [Available online at http://ams.confex.com/ams/pdfpapers/117819.pdf.]

Schafer, R., S. Avery, P. May, D. Rajopadhyaya, and C. Williams, 2002: Estimation of rainfall drop size distributions from dual-frequency wind profiler spectra using deconvolution and a nonlinear least squares fitting technique. *J. Atmos. Oceanic Technol.,* **19,** 864–874.

Scharfenberg, K. A., and Coauthors, 2005: The joint polarization experiment: Polarimetric radar in forecasting and warning decision making. *Wea. Forecasting,* **20,** 775–788.

Shapiro, A., and J. J. Mewes, 1999: New formulations of dual-Doppler wind analysis. *J. Atmos. Oceanic Technol.,* **16,** 782–792.

Smull, B. F., and R. A. Houze Jr., 1987: Dual-Doppler radar analysis of a midlatitude squall line with a trailing region of stratiform rain. *J. Atmos. Sci.,* **44,** 2128–2149.

Straka, J. M., D. S. Zrnić, and A. V. Ryzhkov, 2000: Bulk hydrometeor classification and quantification using polarimetric radar data: Synthesis of relations. *J. Appl. Meteor.,* **39,** 1341–1372.

Wakasugi, K., A. Mizutani, M. Matsuo, S. Fukao, and S. Kato, 1986: A direct method for deriving drop-size distribution and vertical air velocities from VHF Doppler radar spectra. *J. Atmos. Oceanic Technol.,* **3,** 623–629.

Waldteufel, P., and H. Corbin, 1979: On the analysis of single-Doppler radar data. *J. Appl. Meteor.,* **18,** 532–542.

Williams, C. R., 2002: Simultaneous ambient air motion and raindrop size distributions retrieved from UHF vertical incident profiler observations. *Radio Sci.,* **37,** 1024, doi:10.1029/2000RS002603.

Zawadzki, I., W. Szyrmer, C. Bell, and F. Fabry, 2005: Modeling of the melting layer. Part III: The density effect. *J. Atmos. Sci.,* **62,** 3705–3723.

Zhang, G., J. Vivekanandan, and E. A. Brandes, 2001: A method for estimating rain rate and drop size distribution from polarimetric radar measurements. *IEEE Trans. Geosci. Remote Sens.,* **39,** 830–841.